Article | Open Access

Energy Materials

Luo et al. Energy Mater. 2026, 6, 600068 DOI:10.20517/energymater.2026.65

Performance and mechanism of biobased-supported conjugated polymer donor with dual small-molecule acceptors

Houjin Luo[1,#], Linji Yang[1,#], Tingyong Yi[1,#], Misong Zhao[1,#], Guanqi Sun[1], Yuanyuan Kan[1], Guo Li[1], Ke Sun[1], Songlin Cai[1], Ke Xu[3], Junchao Jin[1,*], Xiaofei Wang[2,*], Tao Liu[1,*]

Keywords:
Non-fullerene, organic photocatalyst, photodegradation, sodium pentachlorophenate

Citation: Luo, H.; Yang, L.; Yi, T.; Zhao, M.; Sun, G.; Kan, Y.; Li, G.; Sun, K.; Cai, S.; Xu, K.; Jin, J.; Wang, X.; Liu, T. Performance and mechanism of biobased-supported conjugated polymer donor with dual small-molecule acceptors. *Energy Mater.* **2026**, *6*, 600068. https://dx.doi.org/10.20517/energymater.2026.65

Received: 11 Apr 2026
First Decision: 19 May 2026
Revised: 29 May 2026
Accepted: 10 Jun 2026
Published: 29 Jun 2026

Academic Editor:
Soo Young Kim
Copy Editor:
Fangling Lan
Production Editor:
Fangling Lan

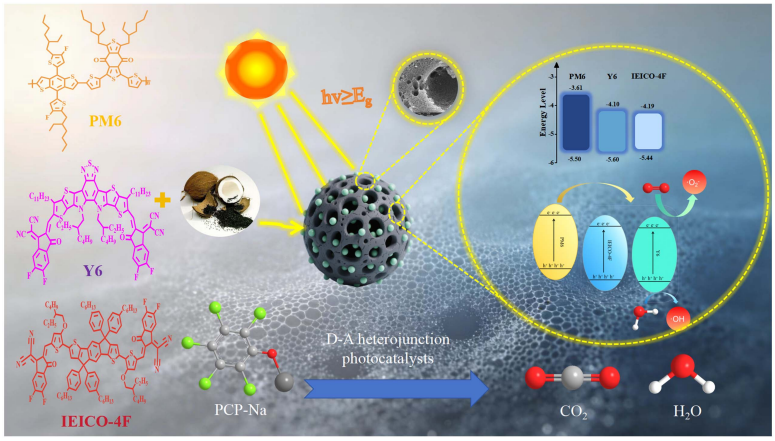

Abstract

Sodium pentachlorophenate (PCP-Na) is a persistent and toxic chlorinated pollutant frequently detected in industrial wastewater. Herein, a fully organic photocatalytic system was developed by integrating coconut shell carbon with organic photovoltaic active-layer materials. A ternary donor-acceptor-acceptor heterojunction (PM6:Y6:IEICO-4F) was constructed to enhance visible-light harvesting and interfacial charge separation. The cascaded energy-level alignment and type-II heterojunction structure broaden light absorption (500-900 nm), suppress carrier recombination, and facilitate charge transfer. Under 300 W xenon lamp irradiation, the optimal photocatalyst achieved 99% degradation of 50 mg/L PCP-Na, within 40 min, and exhibited excellent cycling stability. Superoxide radicals ($\cdot O_2^-$) and photogenerated holes (h^+) are identified as the dominant reactive species, driving stepwise dechlorination and ring-opening processes. This work

[1]School of Chemistry and Chemical Engineering, Guangxi Key Laboratory of Nonferrous Metals and Special Materials Processing, Key Laboratory of New Technologies for Nonferrous Metals and Materials Processing, Ministry of Education, State Key Laboratory of Featured Metal Materials and Life-Cycle Safety for Composite Structures, School of Resources, Environment and Materials, Guangxi University, Nanning 530004, Guangxi, China.
[2]Institute of Eco-Environmental Research, Guangxi Academy of Sciences, Nanning 530007, Guangxi, China.
[3]Shenzhen Institute for Advanced Study, University of Electronic Science and Technology of China, Shenzhen 518110, Guangdong, China.
[#]Authors contributed equally.

[*]**Correspondence to:** Dr. Tao Liu, Dr. Junchao Jin, School of Chemistry and Chemical Engineering, Guangxi Key Laboratory of Nonferrous Metals and Special Materials Processing, Key Laboratory of New Technologies for Nonferrous Metals and Materials Processing, Ministry of Education, State Key Laboratory of Featured Metal Materials and Life-Cycle Safety for Composite Structures, School of Resources, Environment and Materials, Guangxi University, Nanning 530004, Guangxi, China. E-mail: p2025007@gxu.edu.cn; liutaozhx@gxu.edu.cn;

Prof. Xiaofei Wang, Institute of Eco-Environmental Research, Guangxi Academy of Sciences, Nanning 530007, Guangxi, China. E-mail: wangxiaofei26@gxas.cn

reveals that the biochar-supported ternary D-A/A type-II heterojunction enables exceptional visible-light utilization and efficient carrier separation, offering a novel all-organic platform for remediating persistent chlorinated pollutants.

INTRODUCTION

With the rapid development of industry and agriculture, water pollution caused by industrial wastewater discharge, pesticide residues, water source contamination, and inadequate treatment has become a global environmental issue[1]. Many organic wastewater streams also contain various complex halogenated organic compounds that are difficult to remove[2]. Sodium pentachlorophenate (PCP-Na) is one of the most toxic and persistent organic pollutants. It is widely used as an insecticide, herbicide, fungicide, wood preservative, adhesive, paint additive, and in public health applications[3]. It has been detected in surface water, sediments, aquatic organisms, topsoil, and food[4]. Therefore, improper handling of PCP-Na poses serious threats to human health and the ecological environment[5]. Although the application of PCP-Na has declined, PCP-Na pollution remains a environmental issue[6]. Therefore, there is an urgent need to explore effective technological approaches to eliminate the negative impacts of PCP-Na pollutants on ecosystems and human health.

Currently, the primary methods for removing chlorophenol pollutants such as PCP-Na from water domestically and internationally include adsorption[7-10], biological treatment[11-13], extraction[14], Fenton oxidation[15-18], electrochemical methods[2,19], and photocatalytic advanced oxidation processes[20-23]. Adsorption is one of the commonly used techniques for treating chlorophenol water pollution. It captures chlorophenol molecules in water through physical or chemical interactions on the adsorbent surface. This method features simple operation, controllable costs, and recyclability, but it also carries risks such as secondary pollution[24]. Biological treatment of chlorophenol water pollution utilizes microbial metabolic activity to degrade or transform chlorophenol pollutants. Through enzymatic catalysis by microorganisms, it achieves dichlorination, ring-opening, and mineralization. This method is environmentally friendly and cost-effective, but it has drawbacks such as lengthy removal processes, complex degradation mechanisms, and susceptibility of microorganisms to temperature and pH fluctuations[25]. The extraction method for treating chlorophenol water pollution utilizes the principle of like dissolves like. It transfers chlorophenol pollutants from wastewater into an organic phase using an organic solvent (extractant) that is immiscible with water, thereby achieving separation and enrichment[26]. Fenton oxidation for treating chlorophenol water pollution is an advanced oxidation technology based on radical reaction mechanisms. It utilizes the reaction between Fe^{2+} and H_2O_2 to generate highly oxidizing ·OH radicals. Due to the high oxidation potential and non-selective nature of ·OH radicals, they can degrade and oxidize a wide range of organic pollutants[27]. However, in practical applications, it is relatively difficult to control and suffers from drawbacks such as high costs, excessive sludge production, susceptibility to color reversion, and high labor intensity[28]. Unlike these methods, photocatalysis is an environmentally friendly technology that effectively degrades organic pollutants in wastewater by generating strong free radicals such as hydroxyl radicals (·OH) and superoxide anions ($\cdot O_2^-$). Particularly with the development of photocatalysts like graphene-TiO_2 nanocomposites[21] and Bi_3O_4Br[29], it has been widely applied to degrade PCP-Na pollutants in organic wastewater. However, all of the above materials are unmodified photocatalysts. Most inorganic photocatalysts suffer from poor tunability, low recyclability, and narrow absorption ranges, limiting their effectiveness in treating industrial wastewater containing complex organic components[30]. Currently, there is a lack of literature on the degradation of pollutants using organic photocatalysts[31]. Therefore, developing a

green and efficient organic photocatalyst capable of degrading pollutants such as PCP-Na under visible light conditions is crucial for innovative treatment processes targeting PCP-Na and other contaminants in industrial wastewater.

The active layer materials in organic solar cells consist of polymers with conjugated structural systems, incorporating electron donors and electron acceptors. This active layer exhibits high reactivity, an optimal bandgap, and excellent carrier recombination properties, effectively addressing the shortcomings of inorganic catalysts[32]. However, when the charge transport layer of organic solar cells comes into contact with water and oxygen, it becomes damaged, leading to a sharp decline in photovoltaic conversion efficiency. Consequently, active layer materials are rarely directly applied to environmental wastewater treatment. Meanwhile, coconut shell carbon (CSC) has garnered widespread attention due to its porous structure, large surface area, low cost, high availability, surface rich in oxygen-containing functional groups, high mechanical strength, and lack of secondary environmental pollution[33]. To combine the advantages of solar cells with photocatalytic technology, this work utilized CSC with a particle size of approximately 0.25-0.6 mm as the adsorption substrate. Three heterojunction active layers of solar cells, namely PM6:Y6, PM6:IEICO-4F and PM6:Y6:IEICO-4F, were fabricated on substrates via physical blending. Three novel organic semiconductor photocatalytic adsorbents with green property and high efficiency were successfully obtained.

A type-II heterojunction is a typical composite semiconductor structure formed by two or more materials with staggered energy levels. In this structure, the conduction band (CB) of one material is lower in energy than that of the other, while its valence band (VB) is also lower. This staggered arrangement enables photogenerated electrons to transfer from the donor's conduction band to the acceptor's conduction band, and holes to migrate from the acceptor's valence band back to the donor's valence band. Such spatial separation of electrons and holes greatly suppresses carrier recombination, prolongs carrier lifetime, and improves photocatalytic efficiency.

Under the irradiation of a 300 W xenon lamp for 40 min, the degradation rate of PCP-Na by PM6:Y6:IEICO-4F can exceed 99%. In comparison to monomeric organic photocatalytic materials, the D-A type all-organic ternary photocatalytic architecture devised in this investigation is capable of establishing a stepped energy level gradient and fabricating a heterojunction configuration.

In summary, this work combines organic photovoltaic technology with photocatalytic technology, utilizing CSC as the adsorption substrate and organic semiconductors as efficient photocatalytic functional materials, to prepare a novel organic photocatalytic adsorbent with a conjugated polymer-bis-small molecule Acceptors structure. Through various characterization methods, the work investigates the division of labor and synergistic mechanisms between photocatalysis and adsorption. Additionally, liquid chromatography-mass spectrometry (LC-MS) combined with Fukui index explores potential degradation pathways. This approach provides an innovative pathway for the effective removal of PCP-Na and offers a novel research strategy for the photocatalytic degradation of organic pollutants.

EXPERIMENT

Materials

Coconut shells were procured from local markets in Guangxi for preparing the biochar substrate. The pollutant reagents used in this work—PCP-Na—were purchased from TMstandard, while chloroform ($CHCl_3$) was obtained from Merck. Organic semiconductor materials PM6, Y6, and IEICO-4F were purchased from Ossila. All materials used in this experiment were of analytical grade and required no further purification. Deionized water was used for preparing chemical solutions.

Preparation of biochar-based organic photocatalytic composites

The biochar used in this experiment was prepared via physical activation. Briefly, coconut shells were cut and crushed into powder with a particle size of 1-2 mm. After sieving, the powder was placed in a tube furnace. Under a carbon dioxide atmosphere, the temperature was raised to 500 °C at a heating rate of 10 °C/min and maintained for 2 h to improve the porosity, specific surface area, and adsorption capacity of the biochar. After the reaction, the resulting CSC was washed repeatedly with deionized water to remove residual impurities, followed by drying and sieving. CSC with a particle size of approximately 0.25-0.6 mm was selected for subsequent experiments.

Physical blending was employed to fabricate PM6:Y6/CSC, PM6:IEICO-4F/CSC, and PM6:Y6:IEICO-4F/CSC composites. PM6 was mixed individually with Y6, IEICO-4F, and the binary acceptor mixture (Y6:IEICO-4F), respectively, and dissolved in $CHCl_3$ to prepare 10 mL solutions. Each mixture was stirred for 8 h at room temperature (25 °C) in the dark. Subsequently, 5 g of CSC was combined with 10 mL of the organic solution in a 100 mm glass dish. After thorough mixing, the mixture was dried overnight in an oven at 70 °C and collected for further use. For the ternary composite, the mass ratio of PM6, Y6, and IEICO-4F was fixed at 1:1:1.

Adsorption kinetic experiment

The adsorption kinetics experiment was conducted at room temperature. To investigate the adsorption kinetics of PCP-Na, 100 mg of CSC was added to 50 mL of a 50 mg/L PCP-Na solution. During stirring, 5 mL samples of the PCP-Na solution were extracted at regular intervals for concentration measurement. The solution was stirred at 800 rpm. The sampled solutions were filtered using a 0.22 μm pore size microporous membrane. Subsequently, the concentrations of PCP-Na at different time points were measured at 321 nm using a Shimadzu UV-3600 UV-Vis spectrophotometer. The adsorption experiments were simulated using the pseudo-first-order Langmuir kinetics model and the pseudo-second-order Ho-McKay adsorption kinetic model.

Photocatalytic experiment

The photocatalytic process was conducted using a xenon lamp ($\lambda > 420$ nm, 300 W) as the visible light source. A photocatalyst loaded with 100 mg of different organic photovoltaic materials was added to 50 mL of a 50 mg/L PCP-Na solution. The materials in the PCP-Na solution were stirred at 800 rpm to ensure uniform dispersion. At regular intervals, 5 mL of PCP-Na solution was sampled, filtered through a 0.22 μm microporous membrane, and analyzed for concentration using a UV spectrophotometer. The optimal photocatalyst was selected from a series of photocatalysts loaded with different organic semiconductor materials. Subsequently, the effects of varying pH values and pollutant concentrations on the optimal catalyst were investigated. Finally, cyclic repetition tests were conducted to further confirm the reusability of the optimal catalyst. The removal efficiency (η) of PCP-Na was calculated using the equation $\eta = (1 - C/C_0) \times 100\%$, where C_0 is the initial concentration and C is the concentration at the time of sampling.

Quenching experiments

Radical trapping and electron spin resonance (ESR) experiments: To identify key reaction species during pollutant removal, experiments were conducted with isopropanol (20 mmol/L), p-benzoquinone (20 mmol/L), sodium oxalate (20 mmol/L), and $KBrO_3$ (20 mmol/L) were selected as scavengers for ·OH, $\cdot O_2^-$, h^+, and electrons (e^-), respectively. The generation characteristics of $\cdot O_2^-$ and ·OH in the photocatalytic material were measured using a Bruker A300 paramagnetic resonance spectrometer.

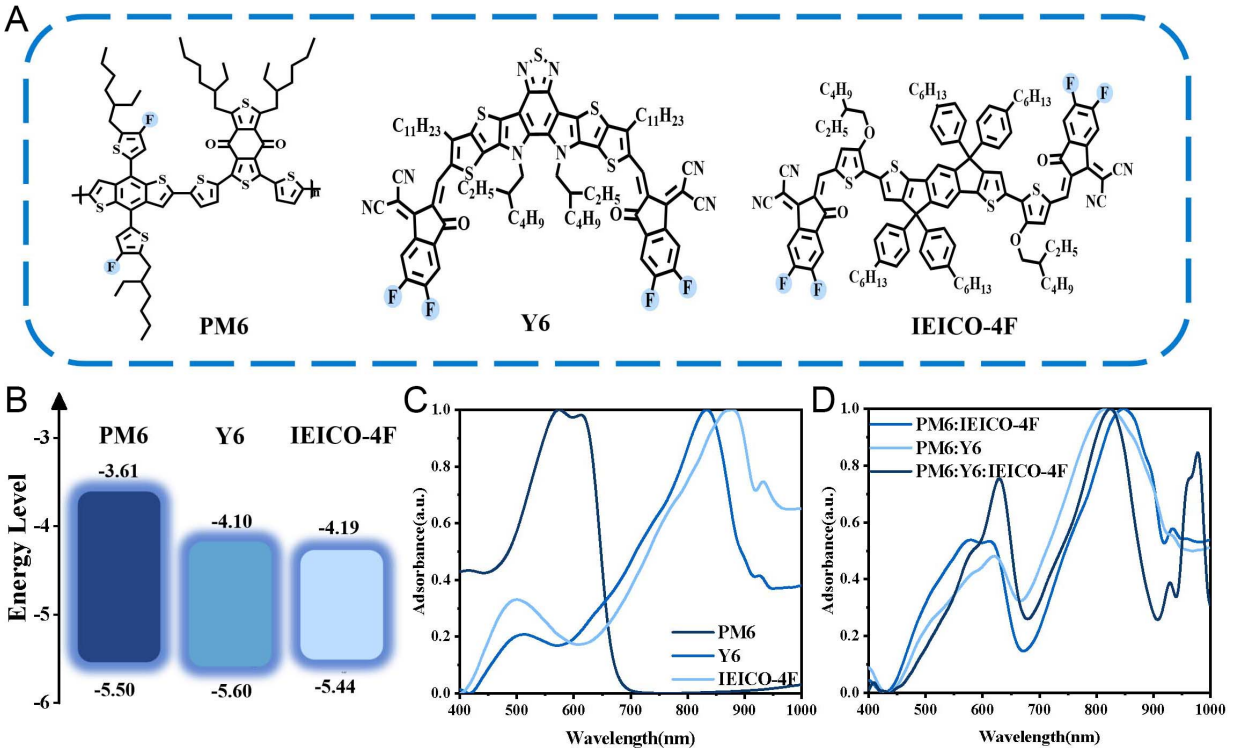

Figure 1. (A) Chemical Formula of PM6, IEICO-4F, Y6, (B) Energy Level Diagram of PM6, IEICO-4F, Y6, (C) Ultraviolet-visible Absorption Spectra of Three Monomer Materials, (D) Ultraviolet-visible Absorption Spectra of Three Photocatalysts.

RESULTS AND DISCUSSION

Physical and chemical properties

Figure 1A shows the structures of several donor and acceptor materials required for this work. PM6 is a novel donor conjugated polymer based on fluorothienyl substituted benzothiophenes. IEICO-4F and Y6 are two non-fullerene organic small-molecule acceptor materials with broad light absorption, tunable frontier molecular orbitals, strong electron-accepting ability, and favorable charge-transport properties. Compared with fullerene materials, non-fullerene small molecule acceptor materials effectively solve the dilemma of limited tunability of absorption range and frontier orbitals of fullerene acceptor to match appropriate electron donor[34,35]. Therefore, this is also an important reason why non-fullerene materials IEICO-4F and Y6 are selected as electron acceptors in this work. As an electron donor, the PM6 molecule contains a planar symmetric BDT unit. This structure strengthens intermolecular π-π stacking and improves charge mobility. Its BDD unit exhibits excellent symmetry and planarity with abundant conjugated skeletons, boosting electron delocalization and constructing efficient charge transport pathways.The Y6 molecule possesses strong electron-withdrawing heteroaromatic groups that facilitate charge transfer. Meanwhile, the BZIC structure reduces steric hindrance, exposing more active sites and elevating photocatalytic performance[36-38]. In contrast, long alkoxy chains on the thiophene ring of IEICO-4F increase molecular steric resistance, which restricts the photocatalytic reaction process.

As illustrated in Figure 1B, Supplementary Figures 1 and 2 within the scope of this research, cyclic voltammetry (CV) was utilized to precisely measure the energy levels of the highest occupied molecular orbital (HOMO) and the lowest unoccupied molecular orbital (LUMO) for the compounds PM6, Y6, and IEICO-4F. The measured HOMO/LUMO energy levels are as follows: PM6 exhibits values of -5.50 eV for HOMO and -3.61 eV for LUMO; Y6 demonstrates -5.60 eV for HOMO and -4.10 eV for LUMO; The energy disparity between the frontier orbitals of donor and acceptor materials engenders a staggered energy level

alignment, thereby facilitating the formation of a Type II heterojunction within the photocatalytic system constructed in this investigation[39]. Guided by the principle of minimum energy, e^- undergo spontaneous transition from the HOMO of the donor to that of the acceptor, while h^+ are conveyed in the converse direction. This charge separation mechanism expedites the spatial segregation of electron-hole pairs, mitigates the likelihood of carrier recombination, and consequently augments the photoelectric conversion efficiency of the photocatalyst. As shown in Supplementary Figure 3, the Mott-Schottky (M-S) analysis results provided further corroboration of the energy level alignment and heterojunction architecture within the system. High-frequency M-S curve fitting, utilizing a saturated calomel electrode (SCE) as the reference, revealed that both Y6 and IEICO-4F exhibited characteristic n-type semiconductor behavior, with their CB positions demonstrating excellent concordance with the LUMO energy levels derived from CV measurements. Integrating the findings from CV and ultraviolet-visible (UV-Vis) spectroscopy, PM6 was confirmed to possess p-type semiconductor properties, thereby establishing a well-defined, stepwise energy level cascade among the three components. Furthermore, the disparity in semiconductor types between the p-type donor and n-type acceptor substantiated the successful formation of a p-n heterojunction within the composite system. This outcome effectively validated the rationality underlying the interface structure engineering and energy level alignment in the all-organic ternary system, offering dual reinforcement—both structural and energetic—for the enhancement of photocatalytic degradation performance[40,41].

Figure 1C and D show the UV-visible absorption spectral characteristics of the monomer material and the composite photocatalyst: the monomeric donor material PM6 exhibits strong absorption in the short-wavelength region at approximately 600 nm, while the acceptor materials Y6 and IEICO-4F extend the absorption edge to the near-infrared region of 800-900 nm. The three materials show typical spectral complementarity in these two wavelength ranges. Compared with individual monomer materials, the absorption spectrum of the ternary composite system PM6:Y6:IEICO-4F effectively integrates the absorption characteristics of the three components. It not only achieves broad spectral coverage across the two bands, which compensates for the absorption blind spots of single materials in either the long-wavelength or short-wavelength regions, but also realizes synergistic enhancement of absorbance in both ranges. This indicates that the ternary composite structure successfully broadens the light absorption range and simultaneously improves the absorption intensity, providing a solid optical and structural basis for optimizing the photoelectric conversion efficiency of organic photovoltaic devices.

In this work, the effect of different donor-acceptor ratios on photocatalytic performance was explored systematically. Composite materials with four different mass ratios of 1:1:1, 1:1:0.5, 0.5:0.5:1 and 1:0.5:0.5 were prepared for comparative research. As can be seen from Supplementary Figure 4, the ternary composite with the ratio of 1:1:1 exhibits the most outstanding photocatalytic activity. Relevant previous studies have demonstrated that equal component proportion can realize effective spectral complementarity between different acceptor materials, which broadens the light response range and enhances light utilization efficiency. Meanwhile, this balanced ratio is conducive to constructing ordered stepped energy level structure, which can greatly promote the separation and migration of photogenerated carriers. Moreover, reasonable component matching can regulate appropriate microphase separation structure and form close interfacial interaction, which effectively suppresses the recombination of e^- and h^+. All these advantages jointly optimize the overall photoelectric properties of the materials and finally achieve superior photocatalytic degradation performance[42-44].

Photoelectric property

In order to further investigate the photogenerated carrier behavior of the three materials, Photoluminescence spectroscopy (PL) and Time-Resolved Photoluminescence (TRPL) spectra of the three photocatalyst materials were measured. The carrier separation and recombination efficiency of the photocatalyst were

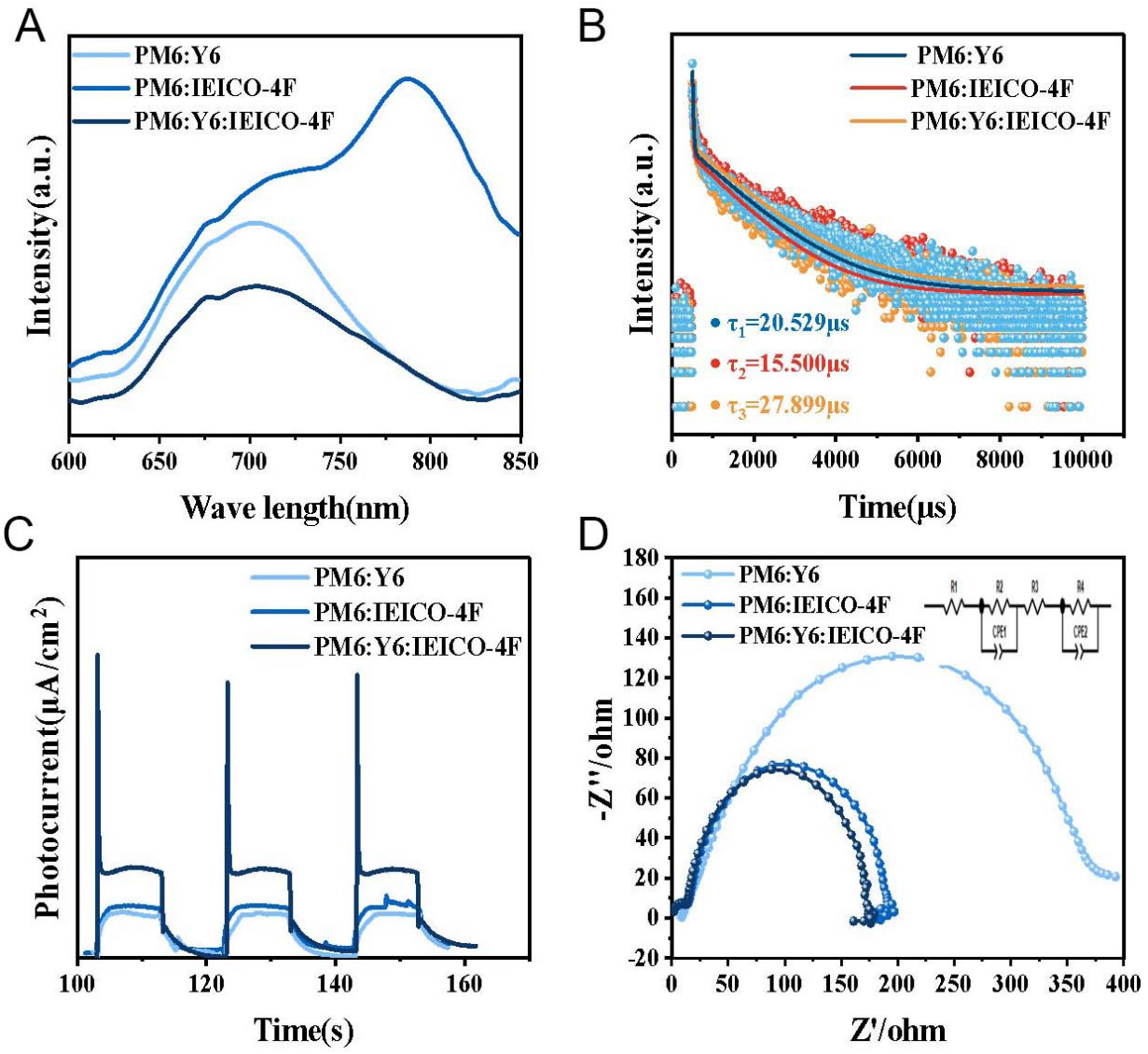

Figure 2. (A) PL spectra of three photocatalysts, (B) TRPL spectra of three photocatalysts, (C) Photocurrent spectra of three photocatalysts, (D) EIS spectra of three photocatalysts.

analyzed by PL spectra. The transient lifetime of the photocatalyst carriers was analyzed by time-resolved PL spectra. As shown in Figure 2A, the peak value of PM6: Y6: IEICO-4F is lower than that of the other two binary photocatalysts PM6: Y6 and PM6: IEICO-4F. This indicates that the ternary photocatalyst PM6: Y6: IEICO-4F produces less photons due to radiative recombination, and the photogenerated carriers are not easy to recombine, so the separation efficiency is higher, and the photoelectric conversion efficiency is higher. As shown in Figure 2B, the carrier lifetime of PM6: Y6: IEICO-4F is calculated to be 27.899 μs, the carrier lifetime of PM6: Y6 is 20.529 μs, and the carrier lifetime of PM6: IEICO-4F is 15.500 μs. Obviously, the carrier lifetime of ternary photocatalyst PM6: Y6: IEICO-4F is longer and the photocatalytic performance is better[45].

In addition, electrochemical measurements were performed to investigate the charge transfer kinetics of the three photocatalysts, and photocurrent measurements were performed to investigate the differences in photoresponse of different materials. The resistance of different materials in charge transfer process was discussed by electrochemical impedance spectroscopy (EIS). As shown in Figure 2C, the photocurrent

density of ternary photocatalyst PM6: Y6: IEICO-4F is higher than that of the other two materials, which indicates that the photogenerated carriers of ternary photocatalyst have stronger response ability to light, and the carrier separation efficiency is higher. At the same time, the carriers are more likely to migrate to the catalyst surface to participate in chemical reactions and improve the degradation performance. As shown in Figure 2D, the Nyquist curve of ternary PM6:Y6:IEICO-4F photocatalyst presents the smallest semicircle diameter. This result reveals its low charge transfer resistance, enabling smoother charge migration. Accordingly, PCP-Na degradation proceeds more readily on the material surface, contributing to enhanced photocatalytic capability. Electrochemical analysis thus verifies the superior performance of the ternary photocatalyst[46,47].

The experimental results show that the performance of the ternary photocatalyst is better than that of the binary system, which is due to the D/A/A double acceptor structure design: the double acceptor material not only provides additional energy level gradient and charge transfer channel, but also realizes the comprehensive improvement of photocatalytic performance through the synergistic expansion of spectral absorption range[48].

Photocatalytic properties

CSC as a typical biomass carbon material, is an ideal substrate material for photocatalytic system because of its low cost, wide source and developed pore structure. In this work, the dark adsorption capacity and equilibrium adsorption capacity of pure CSC and three kinds of composite photocatalytic systems were characterized by Figure 3A-C. The results showed that the equilibrium adsorption capacity of pure CSC decreased after loading photocatalyst. It was speculated that the functional groups of photocatalyst covered the surface of CSC and blocked the pores, resulting in the decrease of adsorption sites. The adsorption kinetics of PCP-Na on pure CSC and the three as-prepared photocatalysts are analyzed using the Langmuir kinetic model. The fitting results (Supplementary Figure 5A-C, Supplementary Tables 1-3) show that the adsorption capacity of all samples increases rapidly in the initial stage and then gradually reaches equilibrium, confirming that the overall adsorption behavior follows the Langmuir kinetic model. Supplementary Figure 5A-C, Figure 3D-F showed that the adsorption and photocatalysis in this system exhibit a distinct staged synergistic effect, and their respective roles and contributions can be clearly distinguished.At the initial reaction stage (0-25 min), adsorption proceeds rapidly, enabling efficient enrichment of pollutants on the catalyst surface and effectively promoting mass transfer, thereby providing favorable conditions for the subsequent photocatalytic reaction.After 25 min, the adsorption rate slows down sharply, and its contribution to pollutant removal is weakened, while photocatalysis gradually becomes the absolutely dominant mechanism for pollutant degradation. All samples gradually reach adsorption saturation within 40-50 min, indicating that the contribution of adsorption is mainly concentrated in the early stage and only serves as pre-concentration and auxiliary mass transfer for pollutants.In contrast, photocatalysis acts as the core contributor throughout the entire illumination period and is the decisive factor for achieving efficient degradation of pollutants.

BET test results [Supplementary Figure 6A and B] show that the specific surface area of pure CSC is 1,011.449 m^2/g, and decreases to 1,003.851 m^2/g after loading PM6: Y6: IEICO-4F, further verifying the coverage effect of photocatalyst on CSC channels. The adsorption isotherm curve shows IV type, which indicates that the material has mesoporous and microporous composite structure.

In conclusion, CSC and composite photocatalytic systems provide abundant adsorption sites and mass transfer channels for pollutants by virtue of high specific surface area and multistage pore structure, which enhance the adsorption performance of materials.

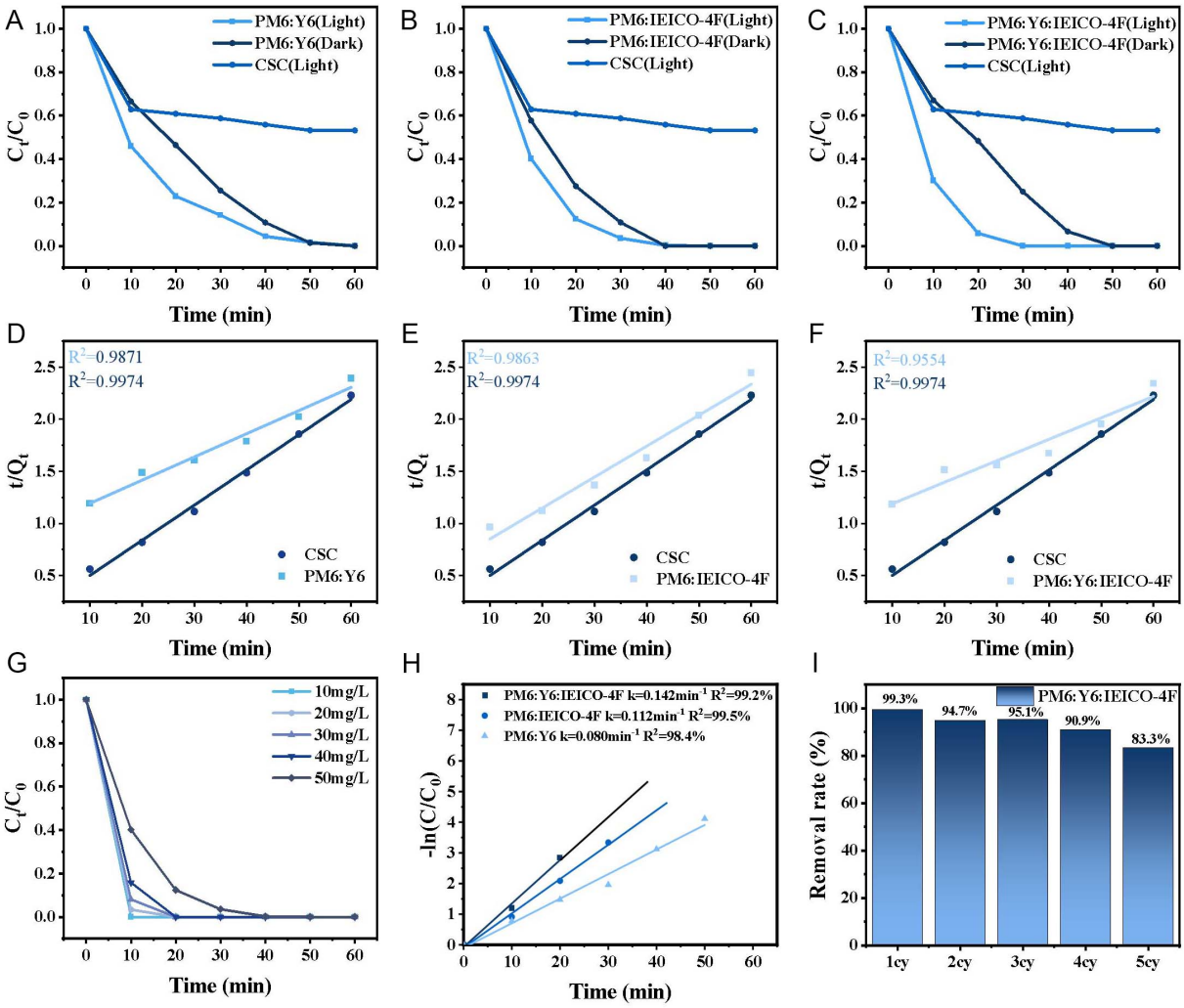

Figure 3. (A-C) Pseudo-second-order kinetic curves of three materials, (D-F) Changes in photodegradation efficiency of PCP-Na over time, (G) Degradation performance of PCP-Na at different PCP-Na concentrations, (H) Linear fitting of adsorption-photocatalytic kinetics for the three catalysts, (I) Degradation performance of PCP-Na using PM6: Y6: IEICO-4F after different cycles.

In order to systematically evaluate the photocatalytic efficiency of D-A type organic heterojunction photocatalyst based on CSC for PCP-Na, a light-dark reaction contrast experiment was designed. Meanwhile, in order to ensure the reliability and comparability of experimental data, the initial concentration of pollutant solution was 50 mg/L in this experiments and subsequent series experiments. Supplementary Figure 7 shows standard calibration curve of PCP-Na solution absorbance *vs.* concentration. Figure 3D-F shows the degradation rate of PCP-Na with time for different photocatalysts. The results show that after 20 min of reaction, the ternary composite photocatalyst PM6: Y6: IEICO-4F can achieve a degradation rate of 74% in the absence of light. When 300 W xenon lamp is introduced as the light source, the degradation rate of the chemical agent can reach 88%, and the catalytic efficiency is improved. Compared with the dark reaction condition, the increase range is as high as 14%. The other two binary catalysts also follow similar rules in the light and dark reaction, which proves that the photocatalytic system constructed in this work improves the degradation performance of PCP-Na. The mechanism can be explained as follows: under the dark reaction condition, the degradation of PCP-Na depends on the excellent adsorption ability of the substrate material CSC, while under the strong light irradiation condition, the adsorption ability and photocatalytic synergy, the photocatalyst produces photogenerated electron-hole pairs at the interface under the light absorption condition, Rapid reaction with oxygen and water to produce a large number of active

species, oxidation and reduction reactions with pollutants at the catalyst surface, and thus improve the overall degradation efficiency[49,50]. At the same time, under the irradiation of 300W xenon lamp for 40 min, the degradation rate of PCP-Na by PM6: Y6: IEICO-4F can exceed 99%, the degradation rate of PCP-Na by PM6: Y6 can reach 94%, and the degradation rate of PCP-Na by PM6: IEICO-4F can reach 96%. Moreover, in Supplementary Figure 8, the PM6: Y6: IEICO-4F composite exhibits high efficiency in photocatalytic degradation of various organic pollutants under visible light irradiation. The excellent photocatalytic performance of PM6: Y6: IEICO-4F system is attributed to its excellent charge separation efficiency and strong light absorption ability in visible light band. Therefore, this further proves that the D-A type organic heterojunction photocatalyst we constructed has huge application advantages and potential in environmental pollution control. However, the photocatalytic performance of the ternary photocatalyst PM6: Y6: IEICO-4F is superior to the other two binary photocatalysts, which also provides strong experimental support for our previous theoretical analysis. At the same time, our organic photocatalytic system shows better photocatalytic performance than reported inorganic photocatalysts. For example, Bi_3O_4Br can reach 92% degradation rate of PCP-Na under xenon lamp irradiation. Graphene/TiO_2 can reach 97% degradation rate of PCP-Na under xenon lamp irradiation. $BWO_{0.12}$ can reach 90% degradation rate of PCP-Na under xenon lamp irradiation[29,51-53]. TiO_2-Sep can reach 90% degradation rate of PCP-Na under xenon lamp irradiation[54]. Therefore, the organic photocatalytic system constructed in this work exhibits better photocatalytic performance. This improvement is mainly attributed to the advantages of our organic photocatalytic system. Its structure is easy to adjust and modify. As a result, its physical properties can be accurately regulated. In addition, the system has a wider spectral absorption range. This allows visible light to be utilized more effectively. At the same time, the organic photocatalytic system we constructed has a large number of π-π conjugated electron systems, strong electron delocalization, large dipole moment of molecules, and can form a stronger built-in electric field. Therefore, the charge transfer resistance is small, and the carrier separation efficiency and photoelectric conversion efficiency are higher.

In order to find the optimal process parameters for degradation of PCP-Na, this work followed the idea of controlling variables and designed the following experiments. PH values has a impact on photocatalytic degradation performance, as shown in Supplementary Figure 9, which shows the change of degradation rate of PCP-Na with the change of pH value. With the decrease of pH value, the removal efficiency of PCP-Na is obviously improved. Under the condition of pH = 3, the removal rate of PCP-Na can reach 99% after 20 min of reaction. This may be attributed to the change of charge distribution on the surface of catalyst under acidic conditions, which enhances the adsorption and enrichment of PCP-Na. As a result, a favorable interfacial environment is created for the reaction between PCP-Na and reactive oxygen species (ROS)[55,56]. At the same time, the concentration of pollutants also has a impact on the degradation efficiency of photocatalyst. As shown in the Figure 3G, under the premise of keeping the dosage of photocatalyst constant (100 mg), the effect of initial PCP-Na concentration (10, 20, 30, 40, and 50 mg/L) on degradation rate was investigated. The results showed that the degradation rate decreased gradually with the increase of pollutant concentration. When the initial concentration was 10 mg/L, the degradation rate of PCP sodium was the fastest, and the degradation rate could reach 99% in only 10 min. This can be attributed to active species produced by photocatalyst PM6: Y6: IEICO-4F and active sites on its surface[57,58]. At low concentrations, pollutants can quickly combine with active species and active sites, while at high concentrations, they form a competitive relationship, resulting in the inhibition of degradation rate. At the same time, although the degradation rate is different under different concentrations, the degradation rate can reach 99% after 40 min, which indicates that the ternary composite photocatalyst constructed in this work has good degradation performance in the wide concentration range of 10-50 mg/L, and the photocatalytic system has good adaptability in different polluted environments. Figure 3H shows the adsorption-photocatalytic degradation kinetic curves for different catalyst dosages. The k values for the degradation of high-concentration PCP-Na with different mass catalysts are 0.080, 0.112, and 0.142/min, respectively. Notably, the kinetic fitting was performed based

on the entire reaction process involving both adsorption and photocatalysis simultaneously, rather than the photocatalytic stage alone. Although adsorption contributes in the initial stage, all kinetic curves still exhibit excellent linearity with high correlation coefficients. This phenomenon originates from the unique synergistic effect between adsorption and photocatalysis: rapid adsorption in the early stage promotes pollutant enrichment and mass transfer, thereby facilitating and matching the subsequent photocatalytic process without disrupting the kinetic behavior. Accordingly, the overall degradation process still follows the pseudo-first-order kinetic model well. Therefore, the rate constants obtained from the entire process are reasonable and comparable, and can quantitatively reflect the comprehensive degradation efficiency of the photocatalysts.

The stability and reusability of photocatalyst are the core indexes to measure its practical application value. In this work, the stability of PM6: Y6: IEICO-4F was evaluated through cyclic degradation experiments, as shown in Figure 3I, which shows the concentration change of PCP-Na under different cycle times. Even after five cycles, the degradation rate of PM6: Y6: IEICO-4F can still maintain a high level of degradation performance of 83.3% after 60 min irradiation by 300 W xenon lamp, and its catalytic efficiency is reduced by about 16%. The gradual attenuation of photocatalytic degradation performance after multiple cycles can be mainly attributed to the continuous accumulation of PCP-Na and its degradation intermediates on the catalyst surface and within the pore structure. These adsorbed by-products progressively cover and block the active sites, reducing the number of available reactive centers and thereby decreasing the photocatalytic reaction rate. In contrast, catalyst regeneration via water washing and drying after each cycle can effectively remove surface-adsorbed contaminants, re-expose active sites, and maintain stable photocatalytic activity. In this work, no regeneration treatment was performed between cyclic experiments, leading to the continuous accumulation of organic residues and the gradual deterioration of photocatalytic performance[59]. This indicates that our photocatalytic system has good stability and recycling performance, and has a high removal rate of PCP-Na.

Possible degradation mechanisms

As mentioned above, ROS (including ·OH, $\cdot O_2^-$ and h^+) generated by the reaction of photocatalyst with oxygen and water react with PCP-Na on the catalyst surface to mineralize it into small molecules, thus achieving effective degradation. In order to explore the active species which play a leading role in the photocatalytic degradation process, the radical trapping experiment was carried out in this work. Figure 4A shows that p-benzoquinone (BQ), sodium oxalate (NaC_2O_4), isopropanol (IPA) and potassium bromide (KBr) were used as trapping agents for $\cdot O_2^-$, h^+, ·OH and electron (e^-) respectively in this experiment. The results showed that the degradation rate of PCP-Na decreased with the addition of free radical scavenger compared with that without free radical scavenger. Specifically, the degradation rate decreased from 99% to 73.3% with the addition of BQ, whereas it decreased slightly from 99% to 95.4% with the addition of NaC_2O_4. Similarly, when IPA or KBr was added, the degradation rate decreased from 99% to 94.2% and 96.5% respectively. These results suggest that superoxide $\cdot O_2^-$ radicals and photogenerated holes synergistically exert strong oxidative capacity.

In order to verify the formation mechanism of active species in the photocatalytic reaction system of ternary photocatalyst PM6: Y6: IEICO-4F, ESR technique was used to characterize the system. 2,2,6,6-Tetramethylpiperidin-1-oxyl (TEMPO) was use as a h^+ trapping agent, while DMPO was use to trap ·OH and $\cdot O_2^-$, respectively. As shown in Figure 4B, a strong characteristic signal can be detected under dark conditions, while the signal intensity is attenuated under light conditions, which confirms that a large number of h^+ are generated in the photocatalytic process. The mechanism is that TEMPO molecule presents strong paramagnetic signal due to unpaired e^- in dark environment, and the h^+ and unpaired e^- annihilate in light condition, resulting in the decrease of signal intensity.

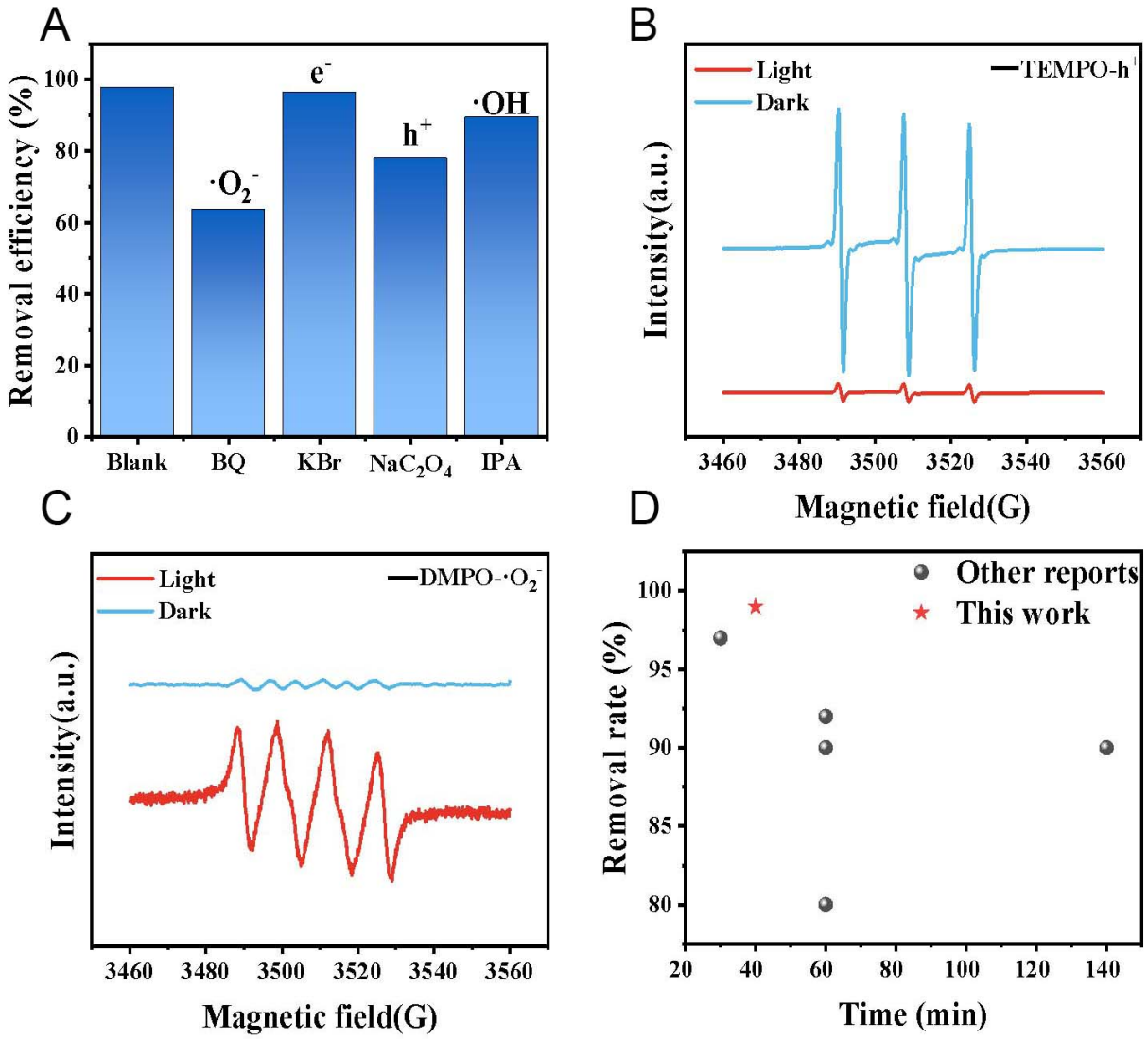

Figure 4. (A) Effects of different radical scavengers on PCP-Na degradation, (B and C) ESR spectra of h^+ and $\cdot O_2^-$, (D) Comparative degradation performance of PCP-Na on different photocatalysts.

In Figure 4C, the results showed that the intensity of paramagnetic signal under light condition was higher than that of dark control group, indicating that a large number of $\cdot O_2^-$ were generated in photocatalytic system.In Supplementary Figure 10, the characteristic signal peak of ·OH is weak, suggesting that ·OH is not the main active species in this reaction system, but it is still generated. The ESR results are consistent with the experimental data of radical scavenging, which confirm the synergistic mechanism of h^+ and $\cdot O_2^-$ in photocatalytic degradation. In Figure 4D, the results showed that comparative degradation performance of PCP-Na on Different Photocatalysts.

The as-fabricated PM6/Y6/IEICO-4F ternary photocatalyst exhibits prominent physical adsorption performance, which provides a favorable prerequisite for efficient pollutant degradation. The material possesses a large specific surface area and abundant hierarchical pore structures, which can expose numerous surface active sites for catalytic reactions. These structural characteristics are well verified by the characterization results of Supplementary Figures 5, 6, and 11. Benefiting from the superior porous structure and surface properties, the composite can effectively adsorb and enrich (PCP-Na) pollutants from aqueous solution onto the catalyst surface. Such enrichment behavior increases the contact probability between

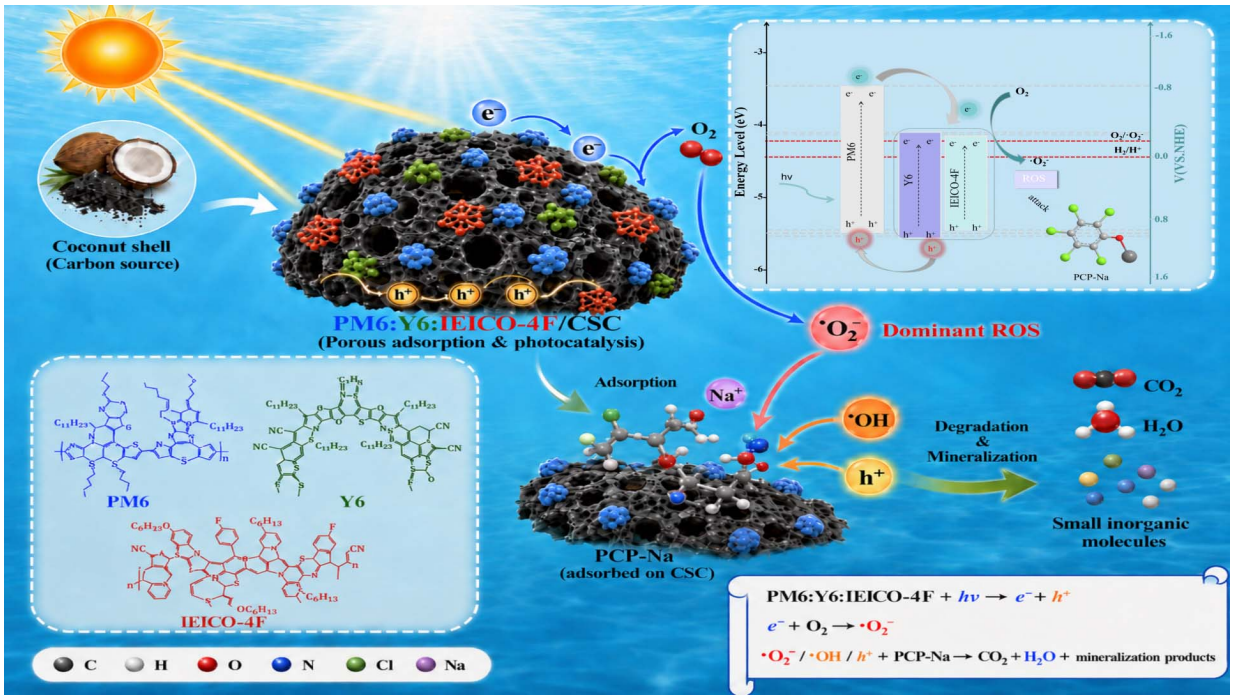

Figure 5. PM6: Y6: IEICO-4F mechanism diagram for degrading PCP-Na.

PCP-Na molecules and active sites, guarantees sufficient reactant concentration for subsequent photocatalytic reactions, and effectively avoids the limitation of low reaction efficiency caused by the low concentration of organic pollutants in water.

During the photocatalytic reaction, the ternary composite system can efficiently harvest visible light and trigger the excitation and separation of photogenerated charge carriers. Under visible light irradiation, the PM6/Y6/IEICO-4F composite undergoes electron energy level transitions to generate abundant photogenerated electron-hole pairs. The constructed type-II heterojunction endows the composite with staggered energy level alignment and a stable built-in electric field, which serves as a powerful driving force for the directional migration and spatial separation of photogenerated carriers. Specifically, the photogenerated electrons on the CB of the PM6 donor migrate directionally to the CBs of the dual acceptors (Y6 and IEICO-4F), while the photogenerated holes on the VBs of the dual acceptors transfer reversibly to the VB of PM6. This efficient spatial separation suppresses the bulk recombination of photogenerated electrons and holes. Furthermore, the unique heterojunction structure prolongs the carrier lifetime and improves charge migration and transmission capacity, enabling abundant electrons and holes to steadily migrate to the catalyst surface and participate in redox reactions.

Energy level analysis further confirms the excellent redox capability of the ternary photocatalytic system. As demonstrated by the energy level results in Figure 5, the conduction band minimum (CBM) potential of Y6 is -0.40 V (*vs.* Normal hydrogen electrode (NHE)), which is more negative than the standard redox potential of the $O_2/\cdot O_2^-$ couple (-0.33 V *vs.* NHE). Such a potential difference endows the composite with sufficient thermodynamic and kinetic feasibility to reduce dissolved oxygen adsorbed on the catalyst surface to produce superoxide radical ($\cdot O_2^-$) active species. Ultimately, the generated $\cdot O_2^-$ radicals cooperate with photogenerated holes to exert strong synergistic oxidation ability, which attacks the PCP-Na molecules enriched on the catalyst surface, destroys their molecular structures, and achieves thorough degradation. The organic pollutants are eventually mineralized into harmless small-molecule products, H_2O, and CO_2, thereby completing the entire photocatalytic degradation process.

Possible degradation pathways

In order to further explore the possible pathway of photocatalytic degradation of PCP-Na, during the experimental process, the contaminated solution at different stages of treatment was retained, and the intermediate products in the degradation process of PCP-Na were detected by LC-MS. Among them, peaks were observed at *m/z* 247.88, 245.86, 231.88 and 211.92. The molecular formula of the intermediate was determined by comparing it with the compound library. See Supplementary Figure 12 for details. Based on this, combined with DFT calculations, two possible degradation pathways of PCP-Na were speculated, as shown in Supplementary Figure 13.

As shown in Figure 6, the initial steps of PCP-Na degradation originate from two different dechlorination processes. In the first pathway, ·OH generated by photocatalytic materials under light conditions first attacks pentachlorophenoxy radical. This radical is highly reactive and easily oxidized by reactive species. Due to the electronegativity and resonance effect of free radicals, the ortho-para position of benzene ring is easily attacked by negatively charged species such as e^- and ·OH[60]. Therefore, photogenerated e^- and ·OH will directly dissociate a chloride ion on the benzene ring to form 2, 3, 5, 6-tetrachlorophenol, 2, 3, 4, 5-tetrachlorophenol or 2, 3, 4, 6-tetrachlorophenol(*m/z* 231.88). After that, ·OH continues to undergo electrophilic substitution reaction, which again dissociates another chloride ion on the benzene ring to form 3, 4, 6-trichloro-1, 2-catechol and 3, 4, 5-trichloro-1, 2-catechol (*m/z* 211.92). At the same time, the $\cdot O_2^-$ in the system can generate ·OH through multi-step reduction reaction. Therefore, O_2^- can also attack the ortho and para positions of PCP-Na benzene ring to generate 2, 3, 5, 6-tetrachloro-1, 4-catechol and 3, 4, 5, 6-tetrachloro-1, 2-catechol (*m/z* 247.88)[29]. Under the strong oxidation of photogenerated h^+, tetrachlorocatechol undergoes dehydrogenation, and hydroxyl groups are oxidized into carbonyl groups to form tetrachloro-o-benzoquinone (*m/z* 245.86). Photogenerated h^+ continuously capture e^- to destroy the conjugated structure of benzene rings, inducing oxidative ring-opening and dechlorination of tetrachloro-o-benzoquinone to produce dichloromaleic acid derivative (*m/z* 183.93). The intermediate further undergoes intramolecular dehydration and cyclization under oxidation of photogenerated h^+, yielding dichloromaleic anhydride (*m/z* 165.92). Dichloromaleic anhydride is then oxidized by photogenerated h^+ with carbon chain cleavage and reconstruction, converting into dihydroxybutyrolactone (*m/z* 118.03). Trichlorocatechol also achieves benzene ring ring-opening, dechlorination and carbon chain rearrangement driven by photogenerated h^+, and finally cyclizes into dihydroxybutyrolactone. Subjected to persistent oxidation attack by photogenerated h^+, chemical bonds of dihydroxybutyrolactone rupture thoroughly and the molecular skeleton decomposes, degrading into oxalic acid[56]. Eventually, it may degrade to carbon dioxide, water and other small molecules. However, no small molecule compounds were detected by liquid mass analysis, presumably due to the low concentration and poor stability of these intermediates in solution[61].

According to the degradation mechanism of PCP-Na, ·OH, $\cdot O_2$- and photogenerated h^+ play vital roles in the photocatalytic degradation process. Based on this, the optimization of heterojunction structure to improve exciton separation efficiency and carrier transport dynamics can effectively inhibit electron-hole recombination behavior and prolong carrier lifetime. The above regulation strategy directly promotes the increase of ROS generation, thus greatly enhancing the photocatalytic degradation effect of PCP-Na. Specifically, type II heterojunctions exhibit a clear carrier directional transport path: e^- migrate from donor PM6 to acceptor Y6 and IEICO-4F under visible light irradiation, while h^+ transfer from acceptor to donor PM6 along the opposite path. The separated e^- and h^+ undergo redox reactions with O_2 and H_2O in the system, respectively, to generate ROS *in situ*, providing a core driving force for bond breaking decomposition and efficient removal of PCP-Na. Meanwhile, the species of ROS generated in the photocatalytic system have been accurately characterized by ESR measurement technique; the preferential attack sites of ROS on PCP-Na molecules have been determined by DFT simulation; the key intermediates in the degradation process of PCP-Na have been successfully verified by LC-MS; and the process of PCP-Na decomposition into smaller

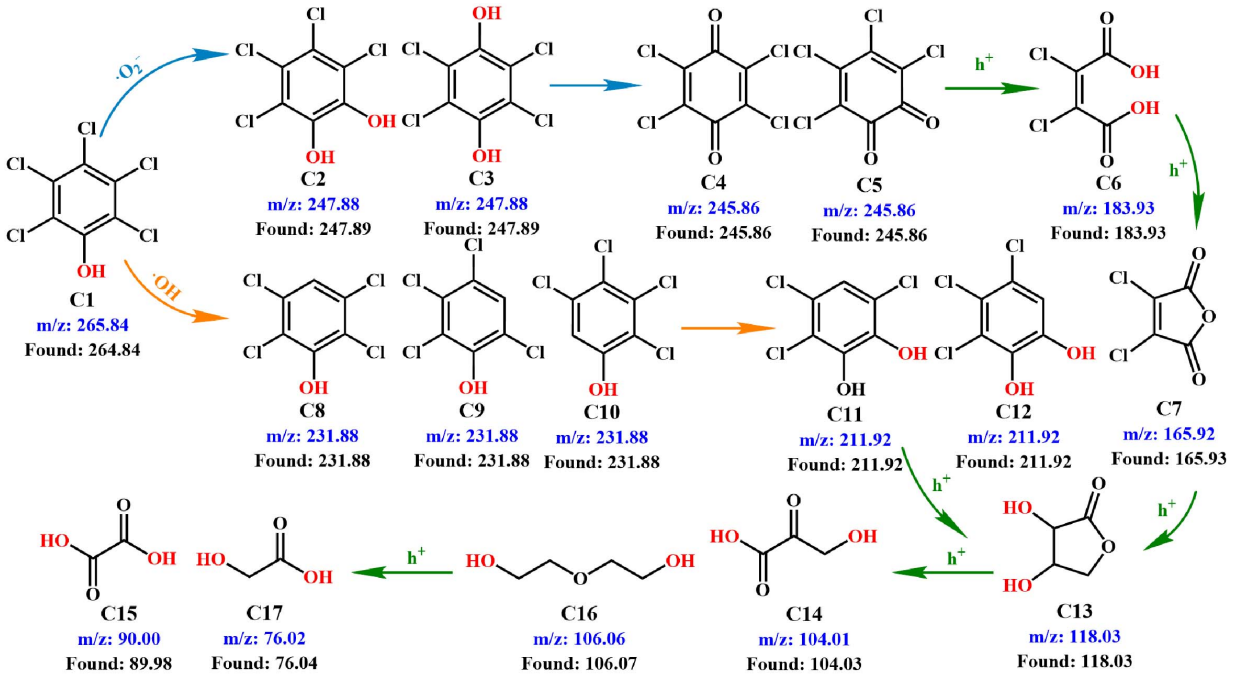

Figure 6. Possible degradation pathways of PCP-Na.

molecules through photodegradation pathway has been comprehensively understood by collaborative characterization and analysis of various technical means.

Figure 7 summarizes the ECOSAR-based QSAR predictions of acute toxicity (a-c) and chronic toxicity (d-f) for PCP-Na and its transformation intermediates (C-series) generated in the PM6:Y6:IEICO-4F system. The figure adopts a heatmap-like encoding to integrate multi-endpoint results, where higher color intensity ("hotter" blocks) corresponds to higher predicted toxicity (i.e., lower effect concentrations such as LC50/EC50 or lower chronic values), whereas lower intensity ("cooler" blocks) indicates reduced toxic potency. From the hotspot distribution, the overall color shift from the parent compound to later intermediates suggests a net attenuation in aquatic toxicity during the degradation sequence, indicating that the photocatalytic transformation tends to reduce ecological hazard as reactions proceed. Nevertheless, the heatmap also reveals endpoint-specific toxicity peaks, demonstrating that risk reduction is not strictly monotonic. In Figure 7A-C, C5 and C7 remain prominent hotspots, particularly toward green algae, implying that certain intermediate structures may transiently retain strong short-term inhibitory potential on primary producers. In Figure 7D-F, C6 and C13 emerge as notable hotspots, suggesting a persistence of long-term sublethal risk (e.g., growth or reproduction impairment) even when acute lethality decreases. Importantly, later-stage products (C14-C17) exhibit predominantly cooler patterns together with markedly reduced mutagenicity, supporting the inference that further transformation drives the system toward less hazardous species. Collectively, Figure 7 demonstrates that PM6:Y6:IEICO-4F can effectively mitigate overall ecotoxicity, while highlighting that mid-stage hotspot intermediates should be considered as key targets for risk control and process optimization.

CONCLUSION

A ternary donor-acceptor-acceptor heterojunction, PM6:Y6:IEICO-4F, was integrated with porous CSC to construct an all-organic photocatalytic system with regulated interfacial energetics and exciton behavior. The dual-acceptor design broadens light harvesting, promotes cascaded energy-level alignment, and facilitates p-n junction formation, thereby generating an internal electric field for directional charge separation.

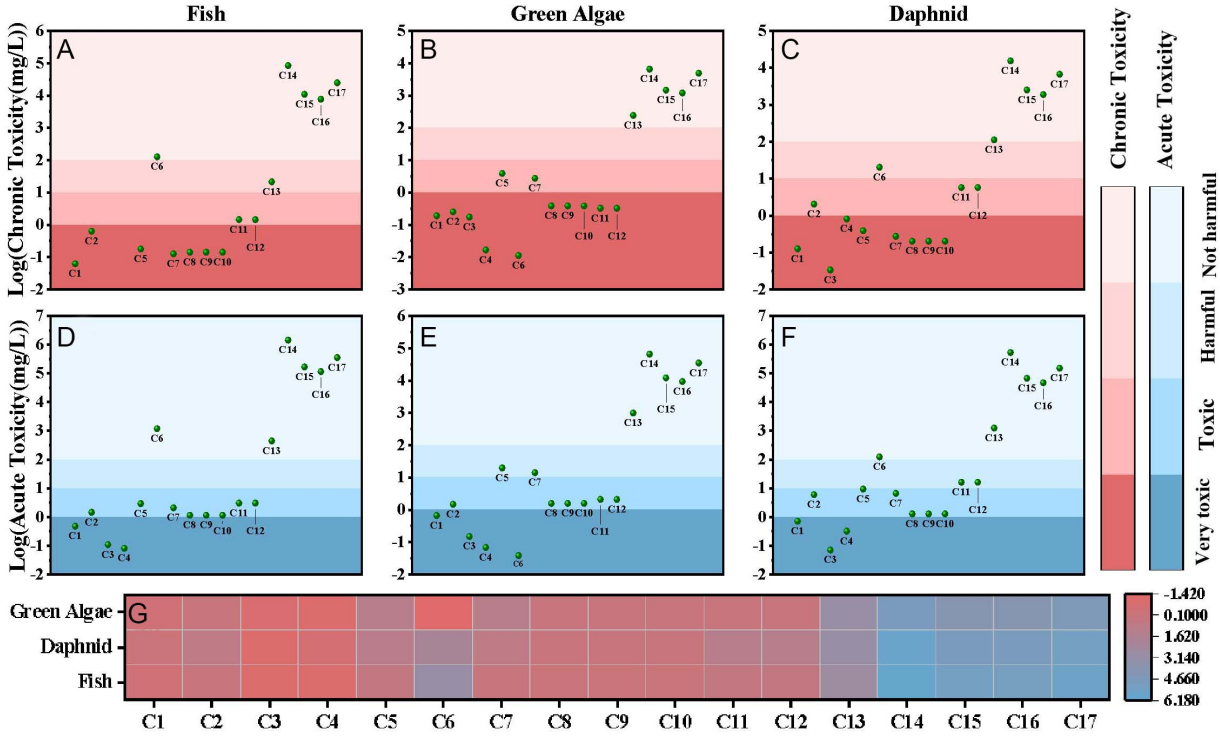

Figure 7. (A-C) Acute toxicity of PCP-Na and its transformation products to fish, green algae and daphnia; (D-F) chronic toxicity of PCP-Na and its transformation products to fish, green algae and daphnia, (G) heatmap of toxicity.

Enhanced photoluminescence quenching, longer carrier lifetime, stronger photocurrent response, and lower interfacial resistance collectively indicate suppressed exciton recombination and accelerated charge transport. Meanwhile, the hierarchical porous CSC framework preserves pollutant adsorption and interfacial reaction coupling, enabling efficient redox processes dominated by ROS and h^+. Overall, this photovoltaic-inspired heterojunction strategy optimizes charge-transfer pathways and provides a promising route for high-performance all-organic photocatalysts.

DECLARATIONS

Authors' contributions

Conceptualization, methodology, funding acquisition: Liu, T.
Writing-original draft, experimental, data analysis: Luo, H.; Yi, T.; Zhao, M.; Sun, G.; Sun, K.
Writing-review & editing: Luo, H.; Yi, T.; Zhao, M.; Yang, L.; Kan, Y.; Xu, K.; Liu, T.
Visualization, software: Yang, L.; Li, G.; Cai, S.; Jin, J.; Wang, X.; Liu, T.
Supervision: Jin, J.; Wang, X.; Liu, T.

Availability of data and materials

The original contributions presented in this study are included in the article/Supplementary Materials. Further inquiries can be directed to the corresponding authors.

AI and AI-assisted tools statement

During the preparation of this manuscript, AI tools including ChatGPT (GPT-5.5, released on April 23, 2026) and Doubao (V13.5.0, released on May 26, 2026) were only applied for the graphical simulation of coconut shell carbon. These AI tools had no involvement in the research design, data collection, data analysis, result interpretation or any scientific content of this work. All authors take full responsibility for the accuracy, integrity, and final content of the manuscript.

Financial support and sponsorship

This work was supported by the Guangxi Science and Technology Major Program (Grant No. Guike

JF2503980030); the Green Utilization of Guangxi's Unique Metal Resources and Research, Development, and Application of New Materials Program (Grant No. Guike AD25069078); and the Open Foundation of the State Key Laboratory of Featured Metal Materials and Life-cycle Safety for Composite Structures (Grant No. MMCS2023OF04).

Conflicts of interest

All authors declared that there are no conflicts of interest.

Ethical approval and consent to participate

Not applicable.

Consent for publication

Not applicable.

Copyright

Supplementary Materials

Supplementary Materials

REFERENCES

1. Nidhi; Renu; Garg, T.; et al. A novel dual-responsive bio-derived magnetic nanocomposite: An excellent catalyst for efficient photodegradation of contaminants and detection of food additive in wastewater. *Chem. Eng. J.* **2023**, *470*, 144218. DOI
2. Guo, Y.; Li, Y.; Wang, Z. Electrocatalytic hydro-dehalogenation of halogenated organic pollutants from wastewater: a critical review. *Water. Res.* **2023**, *234*, 119810. DOI
3. Hu, C.; Zhang, L.; Wang, W.; Cui, Y.; Li, M. Evaluation of the combined toxicity of multi-walled carbon nanotubes and sodium pentachlorophenate on the earthworm Eisenia fetida using avoidance bioassay and comet assay. *Soil. Biol. Biochem.* **2014**, *70*, 123-30. DOI
4. Hopkins, Z. R.; Blaney, L. An aggregate analysis of personal care products in the environment: Identifying the distribution of environmentally-relevant concentrations. *Environ. Int.* **2016**, *92-3*, 301-16. DOI
5. Vollmuth, S.; Zajc, A.; Niessner, R. Formation of polychlorinated dibenzo-p-dioxins and polychlorinated dibenzofurans during the photolysis of pentachlorophenol-containing water. *Environ. Sci. Technol.* **2002**, *28*, 1145-9. DOI
6. Zhang, W.; Tang, Y.; Han, Y.; et al. Immunotoxicity of pentachlorophenol to a marine bivalve species and potential toxification mechanisms underpinning. *J. Hazard. Mater.* **2022**, *439*, 129681. DOI
7. Bi, C.; Zhao, B.; Zheng, W.; et al. Highly efficient adsorption and capture of prevalent phenolic contaminants from the real samples by trifluoromethyl-functionalized covalent organic frameworks. *Sep. Purif. Technol.* **2024**, *339*, 126631. DOI
8. Gao, Y.; Zhu, S.; Mu, M.; Li, D.; Lu, M. Design of magnetic multivariate metal-organic framework for high-efficient adsorption and rapid magnetic separation of bisphenol pollutants. *Chem. Eng. J.* **2023**, *475*, 146459. DOI
9. Ma, X.; Liu, Y.; Zhang, X.; Wei, Y.; Ma, H. Multifunctional SGCG/CuO_2 composite hydrogel for integrated wastewater remediation: Copper ions removal, phenolic pollutant degradation, and bacterial inactivation. *J. Hazard. Mater.* **2025**, *496*, 139486. DOI
10. Zhou, S.; Gu, P.; Wan, H.; et al. Preparation of new triptycene- and pentiptycene-based crosslinked polymers and their adsorption behavior towards aqueous dyes and phenolic organic pollutants. *Sep. Purif. Technol.* **2021**, *278*, 119495. DOI
11. Islam, N. F.; Borah, D.; Saikia, R.; Gogoi, B.; Sarma, H. Microbial dehalogenation of halogenated organic pollutants: a review. *Environ. Chem. Lett.* **2025**, *24*, 101-37. DOI
12. Wang, J.; Zhang, L.; He, Y.; Ji, R. Biodegradation of phenolic pollutants and bioaugmentation strategies: a review of current knowledge and future perspectives. *J. Hazard. Mater.* **2024**, *469*, 133906. DOI
13. Wu, P.; Zhang, Z.; Luo, Y.; Bai, Y.; Fan, J. Bioremediation of phenolic pollutants by algae - current status and challenges. *Bioresour. Technol.* **2022**, *350*, 126930. DOI
14. Soriano, Y.; Andreu, V.; Picó, Y. Pressurized liquid extraction of organic contaminants in environmental and food samples. *TrAC. Trends. Anal. Chem.* **2024**, *173*, 117624. DOI
15. Yin, Y.; Dong, Z.; Li, J.; Yang, J.; Gao, J. Interfacial engineering of Fe-Zr bimetallic oxides boosts phenolic pollutants removal in heterogeneous fenton-like process. *Energy. Environ. Mater.* **2025**, *9*, e70073. DOI

16. Chen, C.; Wang, Y.; Huang, Y.; et al. Overlooked self-catalytic mechanism in phenolic moiety-mediated Fenton-like system: Formation of Fe(III) hydroperoxide complex and co-treatment of refractory pollutants. *Appl. Catal. B. Environ.* **2023**, *321*, 122062. DOI
17. Kantar, C.; Oral, O.; Urken, O.; Oz, N. A. Role of complexing agents on oxidative degradation of chlorophenolic compounds by pyrite-Fenton process: batch and column experiments. *J. Hazard. Mater.* **2019**, *373*, 160-7. DOI PubMed
18. Si, Y.; Guo, Z.; Meng, Y.; et al. Reusing sulfur-poisoned palladium waste as a highly active, nonradical fenton-like catalyst for selective degradation of phenolic pollutants. *Environ. Sci. Technol.* **2021**, *56*, 564-74. DOI
19. Pei, S.; Wang, Y.; You, S.; Li, Z.; Ren, N. Electrochemical removal of chlorophenol pollutants by reactive electrode membranes: scale-up strategy for engineered applications. *Engineering* **2022**, *9*, 77-84. DOI
20. Gusain, R.; Gupta, K.; Joshi, P.; Khatri, O. P. Adsorptive removal and photocatalytic degradation of organic pollutants using metal oxides and their composites: a comprehensive review. *Adv. Colloid. Interface. Sci.* **2019**, *272*, 102009. DOI PubMed
21. Liu, Y.; Xia, P.; Li, L.; et al. In-situ route for the graphitized carbon/TiO_2 composite photocatalysts with enhanced removal efficiency to emerging phenolic pollutants. *Chin. J. Catal.* **2020**, *41*, 1378-92. DOI
22. Peng, W.; Li, D.; Qin, D.; et al. Maximizing singlet oxygen generation: cobalt single-atom advanced oxidation system for efficient and selective degradation of phenolic pollutants in actual waters. *Chem. Eng. J.* **2025**, *519*, 165195. DOI
23. Sheng, Y.; Liu, Y.; Kong, C.; et al. Research progress and future prospects of electrocatalytic degradation of phenolic pollutants in water. *Chem. Eng. J.* **2025**, *525*, 169660. DOI
24. Garba, Z. N.; Zhou, W.; Lawan, I.; et al. An overview of chlorophenols as contaminants and their removal from wastewater by adsorption: a review. *J. Environ. Manag.* **2019**, *241*, 59-75. DOI
25. Tang, Y.; Wang, Y.; Qin, Q.; Xu, Y. Microbial community acclimation via polarity reversal supports extensive dechlorination and anaerobic mineralization of 2,4,6-trichlorophenol in biocathode. *Chem. Eng. J.* **2024**, *500*, 157151. DOI
26. Sas, O. G.; Castro, M.; Domínguez, Á.; González, B. Removing phenolic pollutants using deep eutectic solvents. *Sep. Purif. Technol.* **2019**, *227*, 115703. DOI
27. Sheng, B.; Lin, Y.; Xu, H.; Zhang, J. Accelerating reduction of ferric iron by tourmaline for efficient H_2O_2 activation in removing aqueous organic pollutants. *J. Colloid. Interface. Sci.* **2026**, *704*, 139349. DOI
28. Lai, C.; Shi, X.; Li, L.; et al. Enhancing iron redox cycling for promoting heterogeneous Fenton performance: a review. *Sci. Total. Environ.* **2021**, *775*, 145850. DOI
29. Wang, J.; Yu, Y.; Zhang, L. Highly efficient photocatalytic removal of sodium pentachlorophenate with Bi_3O_4Br under visible light. *Appl. Catal. B. Environ.* **2013**, *136-7*, 112-21. DOI
30. Qi, Y.; Zhang, F. Recent progress on overall water splitting using particulate inorganic photocatalysts with wide visible light utilization. *CCS. Chem.* **2025**, *7*, 3591-605. DOI
31. Blázquez-Moraleja, A.; Cabezuelo, O.; Martinez-Haya, R.; Schmidt, L. C.; Bosca, F.; Marin, M. L. Organic photoredox catalysts: tuning the operating mechanisms in the degradation of pollutants. *Pure. Appl. Chem.* **2023**, *95*, 899-912. DOI
32. Li, X.; Kong, X.; Sun, G.; Li, Y. Organic small molecule acceptor materials for organic solar cells. *eScience* **2023**, *3*, 100171. DOI
33. Deng, Z.; Zhang, Q.; Deng, Q.; Guo, Z.; Seok, I. Modification of coconut shell activated carbon and purification of volatile organic waste gas acetone. *Adv. Compos. Hybrid. Mater.* **2021**, *5*, 491-503. DOI
34. Barth, S.; Bässler, H. Intrinsic photoconduction in PPV-type conjugated polymers. *Phys. Rev. Lett.* **1997**, *79*, 4445-8. DOI
35. Alvarado, S.; Seidler, P.; Lidzey, D.; Bradley, D. Direct determination of the exciton binding energy of conjugated polymers using a scanning tunneling microscope. *Phys. Rev. Lett.* **1998**, *81*, 1082-5. DOI
36. Deibel, C.; Mack, D.; Gorenflot, J.; et al. Energetics of excited states in the conjugated polymer poly(3-hexylthiophene). *Phys. Rev. B.* **2010**, *81*, 085202. DOI
37. Wu, Z.; Chen, Y.; Zhang, L.; et al. A ligand-free direct heteroarylation approach for benzodithiophenedione-based simple small molecular acceptors toward high efficiency polymer solar cells. *J. Mater. Chem. A.* **2021**, *9*, 3314-21. DOI
38. Shoaee, S.; Luong, H. M.; Song, J.; Zou, Y.; Nguyen, T. Q.; Neher, D. What we have learnt from PM6:Y6. *Adv. Mater.* **2023**, *36*, 2302005. DOI
39. Liu, Q.; Vandewal, K. Understanding and suppressing non-radiative recombination losses in non-fullerene organic solar cells. *Adv. Mater.* **2023**, *35*, 2302452. DOI PubMed
40. Guo, F.; Chen, Z.; Huang, X.; et al. Cu_3P nanoparticles decorated hollow tubular carbon nitride as a superior photocatalyst for photodegradation of tetracycline under visible light. *Sep. Purif. Technol.* **2021**, *275*, 119223. DOI
41. Sun, H.; Wang, L.; Guo, F.; et al. Fe-doped g-C_3N_4 derived from biowaste material with Fe-N bonds for enhanced synergistic effect between photocatalysis and Fenton degradation activity in a broad pH range. *J. Alloys. Compd.* **2022**, *900*, 163410. DOI
42. Lee, J. W.; Choi, Y. S.; Ahn, H.; Jo, W. H. Ternary blend composed of two organic donors and one acceptor for active layer of high-performance organic solar cells. *ACS. Appl. Mater. Interfaces.* **2016**, *8*, 10961-7. DOI PubMed

43. Wang, J.; Wang, J.; Zhang, F. Ternary polymer solar cells achieving 11.78% efficiency with two fluorinated non-fullerene acceptors. *Org. Electron.* **2019**, *67*, 253-8. DOI
44. He, C.; Shen, Q.; Wu, B.; et al. Simultaneous improvements in efficiency and stability of organic solar cells via a symmetric-asymmetric dual-acceptor strategy. *Adv. Energy. Mater.* **2023**, *13*, 2204154. DOI
45. Xue, M.; Meng, F.; Ma, Y.; Zhou, S. Growing of ultra-thin Bi_2MoO_6 nanoflowers on Co/N-doped graphitic carbon nanoshells as attractive custom supports: excellent photocatalytic degradation activity for pollutants. *Appl. Surf. Sci.* **2023**, *613*, 156100. DOI
46. Hosseini, S. F.; Seyed Dorraji, M. S.; Rasoulifard, M. H. Boosting photo-charge transfer in 3D/2D TiO_2@Ti_3C_2 MXene/Bi_2S_3 Schottky/Z-scheme heterojunction for photocatalytic antibiotic degradation and H_2 evolution. *Compos. Part. B. Eng.* **2023**, *262*, 110820. DOI
47. Wan Ishak, W. N.; Tan, H. L.; Abu Bakar, N. F.; Radacsi, N.; Lim, Y. P. Electrochemical characterization of Z-scheme charge transfer in biomass-derived ZnO/carbon dots for efficient tetracycline degradation. *RSC. Adv.* **2025**, *15*, 24726-38. DOI PubMed PMC
48. Ding, R.; Wang, S.; Yang, Z.; et al. Ternary strategy for energy loss suppression toward efficient rigid and flexible organic solar cells. *J. Mater. Chem. A.* **2025**, *13*, 33356-64. DOI
49. Liu, C.; Zhang, M.; Gao, H.; et al. Cyclic coupling of photocatalysis and adsorption for completely safe removal of N-nitrosamines in water. *Water. Res.* **2022**, *209*, 117904. DOI
50. Hu, Y.; Zhang, P.; Du, J.; Kim, C.; Han, S.; Choi, W. Bifunctional carbon nitride exhibiting both enhanced photoactivity and residual catalytic activity in the post-irradiation dark period. *ACS. Catal.* **2021**, *11*, 14941-55. DOI
51. Zhang, Y.; Zhou, Z.; Chen, T.; Wang, H.; Lu, W. Graphene TiO_2 nanocomposites with high photocatalytic activity for the degradation of sodium pentachlorophenol. *J. Environ. Sci.* **2014**, *26*, 2114-22. DOI
52. Ge, S.; Li, D.; Cui, Z.; et al. Regulating the relative content of O^{2-} and OH for PCPNa degradation on BiOCl plates with controllable exposed crystal faces and surface oxygen vacancies. *Sep. Purif. Technol.* **2019**, *228*, 115743. DOI
53. Wang, S.; Xiong, Z.; Yang, N.; Ding, X.; Chen, H. Iodine-doping-assisted tunable introduction of oxygen vacancies on bismuth tungstate photocatalysts for highly efficient molecular oxygen activation and pentachlorophenol mineralization. *Chin. J. Catal.* **2020**, *41*, 1544-53. DOI
54. Zhou, F.; Yang, M.; Lu, R.; Yan, C. Simultaneous adsorption-photocatalytic treatment with TiO2-Sep nanocomposites for in situ remediation of sodium pentachlorophenol contaminated aqueous and soil. *Environ. Sci. Pollut. Res.* **2022**, *29*, 39557-66. DOI
55. Pan, Y.; Su, H.; Zhu, Y.; Vafaei, Molamahmood. H.; Long, M. CaO_2 based Fenton-like reaction at neutral pH: Accelerated reduction of ferric species and production of superoxide radicals. *Water. Res.* **2018**, *145*, 731-40. DOI PubMed
56. Zhang, W.; Zhang, L.; Luo, H.; et al. Organic heterojunctions synergize with biochar as catalytic sites for rapid herbicide degradation under natural light. *Surf. Interfaces.* **2024**, *46*, 104182. DOI
57. Huang, A.; He, J.; Huang, C.; et al. Optimizing visible light absorption, exciton dissociation, and charge transfer through the interaction of donor-acceptor materials to enhance xanthate photodegradation. *J. Environ. Manag.* **2025**, *385*, 125681. DOI
58. Zhu, H.; Zhang, C.; Xie, K.; Li, X.; Liao, G. Photocatalytic degradation of organic pollutants over MoS_2/Ag-$ZnFe_2O_4$ Z-scheme heterojunction: revealing the synergistic effects of exposed crystal facets, defect engineering, and Z-scheme mechanism. *Chem. Eng. J.* **2023**, *453*, 139775. DOI
59. Long, M.; Huang, C.; Huang, X.; et al. Efficient photodegradation of carbamazepine by organocatalysts incorporating a third component with a more complementary absorption spectrum. *Mater. Horiz.* **2024**, *11*, 6476-85. DOI
60. Xu, X.; Wang, J.; Chen, T.; et al. Deep insight into ROS mediated direct and hydroxylated dichlorination process for efficient photocatalytic sodium pentachlorophenate mineralization. *Appl. Catal. B. Environ.* **2021**, *296*, 120352. DOI
61. Yan, Z.; Tang, W.; Li, B. Expanding metabolome coverage in LC-MS/MS analysis through hydralazine-based multifunctional derivatization. *Anal. Chem.* **2025**, *97*, 26357-63. DOI PubMed